# Strong Field Multiple Ionization as a Route to Electron Dynamics in a van der Waals Cluster

J. Wu,[1,*] X. Gong,[1] M. Kunitski,[2] F. K. Amankona-Diawuo,[3] L. Ph. H. Schmidt,[2] T. Jahnke,[2] A. Czasch,[2] T. Seideman,[3] and R. Dörner[2,†]

[1]*State Key Laboratory of Precision Spectroscopy, East China Normal University, Shanghai 200062, China*
[2]*Institut für Kernphysik, Goethe Universität, Max-von-Laue-Strasse 1, D-60438 Frankfurt, Germany*
[3]*Department of Chemistry, Northwestern University, 2145 Sheridan Road, Evanston, Illinois 60208, USA*

(Received 16 February 2013; published 20 August 2013)

We study the order in which a strong laser field removes multiple electrons from a van der Waals (vdW) cluster. The $N_2Ar$, with an equilibrium $T$-shaped geometry, contains both a covalent and a vdW bond and serves as a simple yet rich example. Interestingly, the fragmenting double and triple ionizations of $N_2Ar$ with vdW bond breaking are favored when the vdW bond is aligned along the laser field polarization vector. However, the orientation of the covalent bond with respect to the laser field rules the triple ionization when both the covalent and vdW bonds are simultaneously broken. Electron-localization-assisted enhanced ionization and molecular orbital profile-dominated, orientation-dependent ionization are discussed to reveal the order of electrons release from different sites of $N_2Ar$.

DOI: 10.1103/PhysRevLett.111.083003 PACS numbers: 32.80.Rm, 42.50.Hz, 42.65.Re

Strong laser fields effectively lead to multiple ionization of atoms, molecules, and clusters, which, in turn, results in multiple bond breakage, fragmentation, and Coulomb explosion. The microscopic mechanisms of this multiple laser matter interaction have mainly been studied in two size regimes: atoms and small linear molecules, for which the individual sequential ionization steps determine the physics, and extended systems, which are governed by collective effects.

One key ingredient determining the order of ionization events is the binding energy, and a second is the geometry. As the size of the system increases, the ionization potentials for different orbitals and sites become more and more degenerate and the geometry plays an increasingly important role. Two elements of structure have been identified to govern strong field ionization. First, the shape of the orbital strongly influences the ionization probability. This is best established for molecules where the single ionization rate has been found to strongly depend on the angle between the polarization vector of the laser field and the molecular axis, as numerically predicted by the strong field approximation [1] and molecular Ammosov-Delone-Krainov tunneling rate [2], and experimentally demonstrated by probing the profiles [3–5] and the dipole moments [6] of the ionizing orbitals. Second, the multiple ionization rate is found to be strongly enhanced for a molecule oriented along the laser field when the bond stretches to a critical length [7]. Under these conditions a localization of the charge on one site [8,9] and joint action of this charge center together with the light field boost the ionization probability, which is alternatively understood as the charge-resonance enhanced ionization [10,11]. This enhanced ionization scenario has been probed by the directional emission of the fragment ions [12], or the electron with respect to the field vector and molecular orientation [13]. Its role was recently predicted in the strong field ionization of the linear polyatomic molecule acetylene [14]. The vast majority of molecules, however, are nonlinear. Such systems offer much richer dynamics. Here it remains to be discovered which of the above structural effects will be important and in which order and from which sites the complex molecule will lose its electrons. The van der Waals (vdW) clusters, in particular, offer a combination of molecular bonds differing in nature and hence an opportunity to learn about new bonding schemes and electronic dynamics in molecules. In the present work we have chosen the vdW cluster $N_2Ar$ [15,16] as a relatively simple but yet rich example.

Figure 1(a) shows the profile of the highest occupied molecular orbital (see the Supplemental Material [17] for details) of equilibrium $T$-shaped $N_2Ar$ in our laboratory coordinate system, where the rare-gas atom Ar is weakly bound to the diatomic molecule $N_2$ with a bond strength of 12.5 meV and a bond length of 3.7 Å [15]. The vdW bond strength decreases and the bond length grows when the structure deviates from the $T$ shape, reaching 9.3 meV and 4.3 Å, respectively, at the linear geometry [15]. Both the measured vdW bond length ($\sim$3.8 Å) and the coincident three-body breakup imaging [16] indicate the dominance of the $T$-shaped geometry of $N_2Ar$ in our jet.

The experimental set up consists of a low temperature supersonic jet [16,18] of a translational temperature below 5 K. Since the energy spacing between the lowest vibrational states of $N_2Ar$ is rather small, in the range of 10 $cm^{-1}$ [19], the vibrational modes can be efficiently cooled in the jet expansion, leading to a similar or slightly higher vibrational temperature in which we expect that $N_2Ar$ is mostly in the ground vibrational state, as we observed in $Ar_2$ [20] (see the Supplemental Material [17] for more discussion). We produced $N_2Ar$ by coexpanding

 

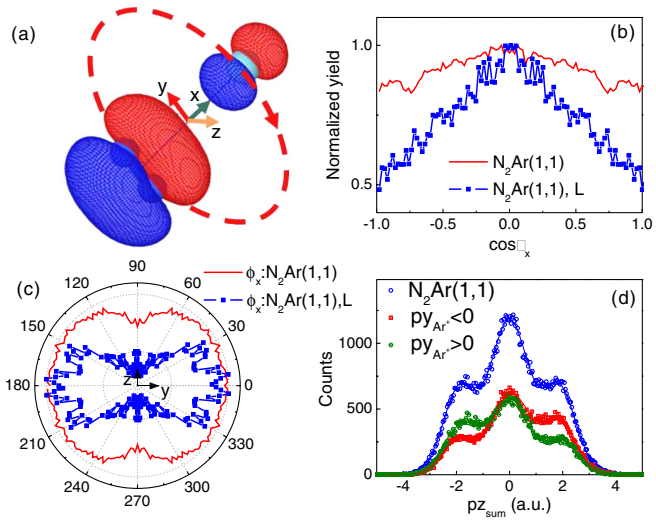


FIG. 1 (color online). (a) Profile of the highest occupied molecular orbital of a $T$-shaped $N_2Ar$ molecule in our laboratory coordinate system. The dashed ellipse shows the polarization $y$-$z$ plane of the clockwise rotating laser field. (b), (c) Angular distributions of $N_2Ar(1, 1)$, $\cos\theta_x$ with respect to the $x$ axis and $\phi_x$ in the $y$-$z$ plane with respect to the $y$ axis, in our elliptically and linearly polarized laser fields. The letter $L$ stands for the linear polarization. (d) Ion sum-momentum distributions of $N_2Ar(1, 1)$ along the $z$ axis for $N_2Ar$ with its vdW bond oriented within a cone of 20° about the $y$ axis. The solid curves are the convolution fits of the sequentially released two electrons.

the 1:1 mixture of $N_2$ and Ar through a 30 $\mu$m nozzle at a driving pressure of 3.5 bar. We estimated a jet density of $\sim 3 \times 10^{10}$ cm$^{-3}$ which consisted of $\sim$1–2% $N_2Ar$ in the interaction region. The molecular beam propagates along the $y$ axis and interacts with elliptically polarized laser pulses (790 nm, 35 fs) which propagate along the $x$ axis and are focused by a concave mirror ($f = 7.5$ cm) inside the chamber. The rates of the clean coincidence signals for the breakup channels following double and triple ionizations were less than 3 and 0.2 Hz, respectively, for a laser repetition rate of 8 kHz. The peak intensity and ellipticity of the pulse are measured to be $I_0 \sim 1.2 \times 10^{15}$ W/cm$^2$ ($\pm$2% fluctuation) and $\varepsilon \sim 0.9$ ($\pm$1% fluctuation), with its major and minor polarization axes along the $y$ and $z$ axes as illustrated in Fig. 1(a), respectively. The Gaussian intensity distribution in the laser focus broadens the momentum distribution of the released electron due to the intensity-dependent streaking by the rotating field, which, however, does not smear out the peaked structure of the sum-momentum distribution, as shown in the following. We applied standard cold target recoil ion momentum spectroscopy [21], where the fragment ions were detected by a time- and position-sensitive microchannel plate detector at the end of the spectrometer.

To learn about the first two steps of the ionization sequence, we start our discussion with the double ionization channel $N_2Ar^{2+} \rightarrow N_2^+ + Ar^+$ [referred to as $N_2Ar(1, 1)$], in which the vdW bond breaks. We describe the bond orientation by its polar ($\theta$) and azimuthal ($\phi$) angles with respect to the $x$, $y$, or $z$ axes in our laboratory coordinate system, where the axial recoil approximation is employed for the two-body Coulomb explosion of the two-sites multiple ionization of $N_2Ar$. The axial recoil approximation may not be satisfied when the dissociation of the molecular ion is accompanied by a fast rotation [22] or intramolecular bending vibrational modes are excited, which is often the case for polyatomic molecules of complex geometry and high temperature. Nonetheless, the axial recoil approximation is successful for breakup processes of the type considered here, where rotation of the vdW cluster is much slower than the rapid fragmentation that follows two-sites multiple ionization [18] and a dominated $T$-shaped geometry. As recently reviewed in Ref. [23], photoelectron angular distributions have been widely used to investigate the rich ionization dynamics of polyatomic molecules, including three-dimensional mapping of a photodissociation process [24], determination of radial dipole matrix elements [25], resolution of the cationic rotational structure [26], and imaging of the geometry of a polyatomic molecule [27]. Here, we explore the orientation-dependent strong-field ionization of a cluster, and the release order of the electrons, by studying the angular distribution of the fragment ions. As shown in Figs. 1(b) and 1(c), the $N_2Ar(1, 1)$ channel is favored when the vdW bond is aligned in the polarization plane and along the major polarization axis. We confirmed this vdW bond orientation in an experiment using linear polarization, which showed an even narrower angular distribution along the light polarization, as shown in Figs. 1(b) and 1(c) (blue square curves).

To trace the electron ejection order, we make use of the angular streaking [28,29] of a close-to-circular light, which encodes the laser field direction and intensity at the instant of ionization to the momenta of the detected electrons. For instance, in our clockwise rotating light, the electrons released when the instantaneous laser field points in the $-y$ (or $+y$) direction will receive a final momentum along $+z$ (or $-z$) if one considers solely the driving by the rotating laser field [30]. For molecules, the rotating strong field acceleration of electrons has been used to uncover ionization from multiple orbitals [4,5], to probe dipole moment of the ionizing orbital [6], to reveal the ionization instant and the initial momentum of the freed electron [31], and very recently to understand the role of phase in chemical bond breaking [32]. As our laser pulse is elliptical, recollision is excluded and multiple ionizations proceed sequentially. The sum-momentum distribution of the sequentially emitted electrons is the convolution of the individual electron momentum distributions. By momentum conservation, this electron sum momentum is imprinted on the sum momentum of the correlated ions [5,13,30], allowing us to determine the former by

measuring the latter. Since the strong-field ionization dynamics of a molecule strongly depend on its bond orientation with respect to the light polarization vector due to the orbital profiles and molecular geometries, we are able to reveal the details of each ionization step by extracting the orientation of $N_2Ar$ along a given angle with respect to the laser field vector at the ionization moment.

Figure 1(d) shows the ion sum momentum along the $z$ direction (i.e., $pz_{\mathrm{sum}}$, where our apparatus has the best momentum resolution). Electron emission along $z$ corresponds to the release of the electrons by the instantaneous laser field along $y$. To investigate the $N_2Ar$ with its vdW bond oriented along $y$, we select fragment ions within a cone of 20° about the $y$ axis. The ion sum-momentum distribution [Fig. 1(d)] shows a symmetric three-peak structure (blue open circles). This three-peak structure reflects four possible sum momenta of the sequentially released two electrons [5,13]. We fit this distribution by convoluting two Gaussians [see Eq. (1) in Refs. [5,13]], obtaining for the most likely momenta of the first and second electrons $pz_{\mathrm{e1}} = 0.77$ a.u. and $pz_{\mathrm{e2}} = 1.09$ a.u. For circularly polarized light these momenta are directly given by the instantaneous field strength at the instant of the electron release. This result shows that the second electron is released at higher laser intensity, i.e., later in the pulse than the first one. The $pz_{\mathrm{sum}}$ distribution becomes asymmetric when we gate on the departing direction of $Ar^+$ to $+y$ or $-y$ [see Fig. 1(d)], indicating that $N_2Ar(1, 1)$ is created preferentially when the laser field points from Ar to $N_2$ ($\sim 1.4$ times of that by a laser field pointing from $N_2$ to Ar).

Insight into the fundamental physics underlying our experimental results is gained through two types of calculations—the shapes and energies of the molecular orbitals, and population analysis (charge distributions) within the Mulliken, charges from the electrostatic potential on a grid (ChElPG), and natural bond orbital (NBO) approaches. Details of our methods and results are provided in the Supplemental Material [17]. We remark here only that both types of calculations show that the cluster orbitals are mostly localized about either the Ar or the $N_2$ center, while the population analysis illustrates also the charge distribution across the cluster in differently charged states. We thus expect the first electron ejection to be symmetric with respect to the Ar-$N_2$ axis. The laser field- and molecular orientation-dependent release of the second electron are then ruled by the electron-localization-assisted enhanced ionization [13]. The equilibrium length of the vdW bond for $N_2Ar$ lies already in the critical range, and therefore bond stretching is not needed to observe the enhanced ionization phenomenon. Although the single ionization potential of $N_2$ is very similar to that of Ar, as demonstrated in Ref. [33], the tunneling single ionization rate of Ar is higher than that of $N_2$ at the same laser intensity. The single ionization probability of $N_2$ is about 3 times lower for a molecule oriented perpendicular to the laser field than that parallel to it [3], due to the shape of the ionizing orbital. This is equivalent to a higher effective ionization potential for orthogonally orientated $N_2$. For the equilibrium $T$-shaped $N_2Ar$ this means that, when the vdW bond is parallel to the laser field, the first electron is more likely to be ejected from the Ar site than from the $N_2$ that mostly lies perpendicular to the field. The second electron is then due to the enhanced ionization mechanism ejected from the up-field $N_2$ site when the laser field points from Ar to $N_2$, as observed in our experiment.

In the following, we discuss the release of the third electron, leading to $N_2Ar^{3+} \rightarrow N_2^+ + Ar^{2+}$, or $N_2^{2+} + Ar^+$, or $N^+ + N^+ + Ar^+$ which we will refer to as $N_2Ar(1, 2)$, $N_2Ar(2, 1)$, and $N_2Ar(1, 1, 1)$, respectively. The relative probabilities of producing these three channels following triple ionization of $N_2Ar$ by elliptical polarized laser pulses are measured in our experiment to be 54%, 24%, and 22%, respectively. Similar to $N_2Ar(1, 1)$, both $N_2Ar(1, 2)$ and $N_2Ar(2, 1)$ are mostly created with the vdW bond oriented along the major polarization axis in the polarization plane, as revealed by the corresponding angular distributions in Figs. 2(a) and 2(b). The much higher yield of $N_2Ar(1, 2)$ compared to $N_2Ar(2, 1)$ results from the lower ionization potential of $Ar^+$ compared to the orthogonal $N_2^+$ (similar to the orientation-dependent single ionization rate of $N_2$ [3,33]).

Figures 2(c) and 2(d) show the sum-momentum distribution $pz_{\mathrm{sum}}$ of the $N_2Ar(1, 2)$ and $N_2Ar(2, 1)$ channels, where $N_2Ar$ with its vdW bond oriented around the $y$ axis is selected for the orientation-dependent analysis. In addition to the recoil momentum the ions receive from the first two ionization steps, the third ionization step adds a

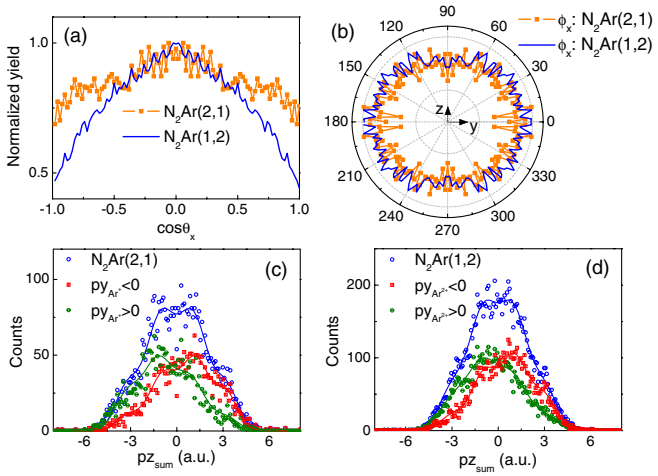


FIG. 2 (color online). (a),(b) Angular distributions of $N_2Ar(2, 1)$ and $N_2Ar(1, 2)$ in our elliptically polarized laser field. (c), (d) Ion sum-momentum distributions of $N_2Ar(2, 1)$ and $N_2Ar(1, 2)$ along the $z$ axis for $N_2Ar$ with its vdW bond oriented within a cone of 20° about the $y$ axis. The solid curves are the convolution fits of the sequentially released three electrons.

momentum $pz_{e3}$ in $+z$ or $-z$ direction, depending on the orientation of the field at the instant of the third tunneling. Thus the sum-momentum distribution for the triply charged ions is a convolution of the three peak structure shown in Fig. 1(d) with a Gaussian distribution of the third electron centered at $+pz_{e3}$ or $-pz_{e3}$. It can be expressed as

$$pz_{\mathrm{sum}}(pz) = \frac{1}{\sqrt{2\pi}} \sum_{i,j,k=+,-} \frac{A_{123ijk}}{\sigma_{123ijk}} \times \exp[-0.5(pz - pz_{123ijk})^2/\sigma^2_{123ijk}], \quad (1)$$

where $A_{123ijk} = A_{1i} \times A_{2j} \times A_{3k}$, $\sigma^2_{123ijk} = \sigma^2_{1i} + \sigma^2_{2j} + \sigma^2_{3k}$, $pz_{123ijk} = -(ipz_{e1} + jpz_{e2} + kpz_{e3})$. By assuming that $N_2Ar(1, 2)$ and $N_2Ar(2, 1)$ are both produced through the intermediate charge state $N_2Ar(1, 1)$, we retrieve from the convolution fits the momenta of the third electron to be $pz_{e3} = 1.11$ and 1.33 a.u., respectively, for $N_2Ar(1, 2)$ and $N_2Ar(2, 1)$. The release of the third electron to create $N_2Ar(2, 1)$ thus occurs at much higher laser intensity than that for $N_2Ar(1, 2)$. This is consistent with the higher effective ionization potential of orthogonal $N_2^+$ as compared to $Ar^+$ and the therefore lower yield of $N_2Ar(2, 1)$.

By gating the direction of departure of $Ar^+$ or $Ar^{2+}$ to $+y$ or $-y$, as shown in Figs. 2(c) and 2(d), noticeable asymmetries in the ion sum-momentum distributions are observed for both $N_2Ar(2, 1)$ and $N_2Ar(1, 2)$ channels. For $N_2Ar(2, 1)$, produced by the electron localization-assisted enhanced ionization [13] when the vdW bond is oriented along the laser field, the third ionization step preferentially occurs when the laser field points from $Ar^+$ to $N_2^+$, i.e. from the up-field potential well. For $N_2Ar(1, 2)$, however, the same enhanced ionization scenario predicts that tunneling of the third electron should be favored with the laser field pointing from $N_2^+$ to $Ar^+$, which is opposite to our experimental observation, as shown in Fig. 2(d). It might be an indication of multielectron effects, as recently observed in multiple ionization of $I_2$ [34]. We note, however, that contrary to the $N_2Ar(2, 1)$ channel, for the $N_2Ar(1, 2)$ channel the momenta of the third ($pz_{e3} = 1.11$ a.u.) and second ($pz_{e2} = 1.09$ a.u.) electrons are very similar, indicating that the second and third electrons are emitted very close in time.

Finally, we discuss the three-body breakup channel of $N_2Ar(1, 1, 1)$, which allows us to directly access the orientations of both the covalent and the vdW bonds by analyzing the relative momenta of the $(N^+, N^+)$ pair and the departing $Ar^+$. To that end we select only events from direct three-body breakup [16]. The angular distributions of the $(N^+, N^+)$ pair and the $Ar^+$ ion [Figs. 3(a) and 3(b)] show that the $N_2Ar(1, 1, 1)$ is mostly created with the covalent bond of the contained $N_2$ oriented along the major polarization axis in the polarization plane and the vdW bond along the propagation direction of the laser pulse, i.e., in the geometry depicted in Fig. 1(a). Using the

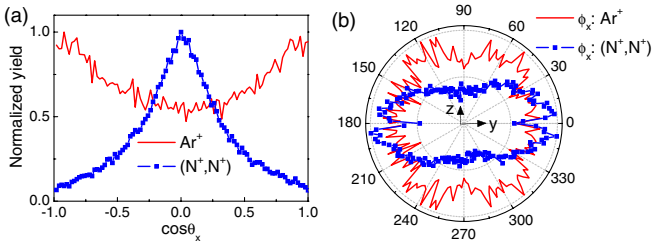


FIG. 3 (color online). (a),(b) Angular distributions of the $(N^+, N^+)$ pair (blue) and $Ar^+$ (red) from $N_2Ar(1, 1, 1)$ in our elliptically polarized laser field.

centroid of the kinetic energy release of the $(N^+, N^+)$ pair ($\sim 12.04$ eV, as calculated from their relative momentum, which disregards the recoil momentum of $Ar^+$), we estimated the N-N distance at the instant of ionization to be $\sim 1.2$ Å, which is much smaller than the critical distance [7,8,11] observed in the intensively studied electron-localization-assisted enhanced ionization of the $N_2$ molecule. One potential scenario to produce the $N_2Ar(1, 1, 1)$ channel is the double ionization and dissociation of $N_2$ to $(N^+, N^+)$ followed by ionization of the remaining Ar atom. As expected from the shape of the ionized orbital, the electron tunneling probabilities strongly depend on the laser field distribution. The orientation of the covalent bond with respect to the laser field dominates the three-body breakup channel of $N_2Ar(1, 1, 1)$. For our elliptically polarization light, $N_2Ar(1, 1, 1)$ is mostly created with the covalent bond in the polarization plane and hence the vdW bond perpendicular to it, conserving the equilibrium $T$-shaped structure of $N_2Ar$.

In summary, we have probed the orientation-dependent strong field ionization of a vdW cluster of $N_2Ar$, containing orthogonal covalent and vdW bonds. The orientations of different bonds with respect to the laser field polarization vectors alter their roles in producing various channels. On the one hand our results point to the possibility of controlling the ionization dynamics of complex molecules by prealigning the neutral species using the well-established method of nonadiabatic alignment and three-dimensional alignment in moderately intense laser fields [35]. On the other hand, our results suggest the potential of multielectron ionization experiments as a probe of the electronic structure and electron dynamics in complex molecules.

This work was supported by the Deutsche Forschungsgemeinschaft, the Program for Professor of Special Appointment (Eastern Scholar) at Shanghai Institutions of Higher Learning and for NCET in University (NCET-12-0177), the Projects from the Shanghai Science and Technology Commission (13QH1401400), the "Shu Guang" project (12SG25), and the Program of Introducing Talents of Discipline to Universities (B12024). T. S. is grateful to the U.S. Army Research Office (W911NF-11-0297) and the U.S. Department of Energy (DE-FG02-04ER15612) for support of this research.

*jwu@phy.ecnu.edu.cn
†doerner@atom.uni-frankfurt.de

[1] J. Muth-Böhm, A. Becker, and F. H. M. Faisal, Phys. Rev. Lett. **85**, 2280 (2000).
[2] X. M. Tong, Z. X. Zhao, and C. D. Lin, Phys. Rev. A **66**, 033402 (2002).
[3] D. Pavičić, Kevin F. Lee, D. M. Rayner, P. B. Corkum, and D. M. Villeneuve, Phys. Rev. Lett. **98**, 243001 (2007).
[4] H. Akagi, T. Otobe, A. Staudte, A. Shiner, F. Turner, R. Dörner, D. M. Villeneuve, and P. B. Corkum, Science **325**, 1364 (2009).
[5] J. Wu, L. Ph. H. Schmidt, M. Kunitski, M. Meckel, S. Voss, H. Sann, H. Kim, T. Jahnke, A. Czasch, and R. Dörner, Phys. Rev. Lett. **108**, 183001 (2012).
[6] L. Holmegaard, J. L. Hansen, L. Kalhøj, S. L. Kragh, H. Stapelfeldt, F. Filsinger, J. Küpper, G. Meijer, D. Dimitrovski, M. Abu-samha, C. P. J. Martiny, and L. B. Madsen, Nat. Phys. **6**, 428 (2010).
[7] K. Codling, L. J. Frasinski, and P. A. Hatherly, J. Phys. B **22**, L321 (1989).
[8] T. Seideman, M. Yu. Ivanov, and P. B. Corkum, Phys. Rev. Lett. **75**, 2819 (1995).
[9] E. Constant, H. Stapelfeldt, and P. B. Corkum, Phys. Rev. Lett. **76**, 4140 (1996).
[10] T. Zuo and A. D. Bandrauk, Phys. Rev. A **52**, R2511 (1995).
[11] S. Chelkowski and A. D. Bandrauk, J. Phys. B **28**, L723 (1995).
[12] K. J. Betsch, D. W. Pinkham, and R. R. Jones, Phys. Rev. Lett. **105**, 223002 (2010).
[13] J. Wu, M. Meckel, L. Ph. H. Schmidt, M. Kunitski, S. Voss, H. Sann, H. Kim, T. Jahnke, A. Czasch, and R. Dörner, Nat. Commun. **3**, 1113 (2012).
[14] E. Lötstedt, T. Kato, and K. Yamanouchi, Phys. Rev. A **85**, 041402(R) (2012).
[15] C. R. Munteanu, J. L. Cacheiro, and B. Fernández, J. Chem. Phys. **121**, 10419 (2004), and references therein.
[16] J. Wu, M. Kunitski, L. Ph. H. Schmidt, T. Jahnke, and R. Dörner, J. Chem. Phys. **137**, 104308 (2012), and references therein.
[17] See Supplemental Material at http://link.aps.org/supplemental/10.1103/PhysRevLett.111.083003 for detailed discussion of the jet temperature, orbital calculation, and population analysis.
[18] J. Wu, A. Vredenborg, B. Ulrich, L. Ph. H. Schmidt, M. Meckel, S. Voss, H. Sann, H. Kim, T. Jahnke, and R. Dörner, Phys. Rev. A **83**, 061403(R) (2011).
[19] G. A. Ayllón, J. Santamaria, S. Miller, and J. Tennyson, Mol. Phys. **71**, 1043 (1990), and references therein.
[20] B. Ulrich, A. Vredenborg, A. Malakzadeh, L. Ph. H. Schmidt, T. Havermeier, M. Meckel, K. Cole, M. Smolarski, Z. Chang, T. Jahnke, and R. Dörner, J. Phys. Chem. A **115**, 6936 (2011).
[21] J. Ullrich, R. Moshammer, A. Dorn, R. Dörner, L. Ph. H. Schmidt, and H. Schmidt-Böcking, Rep. Prog. Phys. **66**, 1463 (2003).
[22] T. Weber, O Jagutzki, M. Hattass, A. Staudte, A. Nauert, L. Schmidt, M. H. Prior, A. L. Landers, A. Bräuning-Demian, H. Bräuning, C. L. Cocke, T. Osipov, I. Ali, R. D. Muiño, D. Rolles, F. J. García de Abajo, C. S. Fadley, M. A. VanHove, A. Cassimi, H. Schmidt-Böcking, and R. Dörner, J. Phys. B **34**, 3669 (2001).
[23] K. L. Reid, Mol. Phys. **110**, 131 (2012).
[24] M. Yamazaki, J. Adachi, T. Teramoto, A. Yagishita, M. Stener, and P. Decleva, J. Phys. B **42**, 051001 (2009).
[25] Paul Hockett, Michael Staniforth, K. L. Reid, and D. Townsend, Phys. Rev. Lett. **102**, 253002 (2009).
[26] P. Hocketty, M. Staniforth, and K. L. Reid, Mol. Phys. **108**, 1045 (2010).
[27] J. B. Williams, C. S. Trevisan, M. S. Schöffler, T. Jahnke, I. Bocharova, H. Kim, B. Ulrich, R. Wallauer, F. Sturm, T. N. Rescigno, A. Belkacem, R. Dörner, Th. Weber, C. W. McCurdy, and A. L. Landers, Phys. Rev. Lett. **108**, 233002 (2012).
[28] P. Eckle, A. Pfeiffer, C. Cirelli, A. Staudte, R. Dörner, H. G. Muller, M. Büttiker, and U. Keller, Science **322**, 1525 (2008).
[29] A. N. Pfeiffer, C. Cirelli, M. Smolarski, R. Dörner, and U. Keller, Nat. Phys. **7**, 428 (2011).
[30] J. Wu, M. Meckel, S. Voss, H. Sann, M. Kunitski, L. Ph. H. Schmidt, A. Czasch, H. Kim, T. Jahnke, and R. Dörner, Phys. Rev. Lett. **108**, 043002 (2012).
[31] M. Odenweller, N. Takemoto, A. Vredenborg, K. Cole, K. Pahl, J. Titze, L. Ph. H. Schmidt, T. Jahnke, R. Dörner, and A. Becker, Phys. Rev. Lett. **107**, 143004 (2011).
[32] J. Wu, M. Magrakvelidze, L. P. H. Schmidt, M. Kunitski, T. Pfeifer, M. Schöffler, M. Pitzer, M. Richter, S. Voss, H. Sann, H. Kim, J. Lower, T. Jahnke, A. Czasch, U. Thumm, and R. Dörner, Nat. Commun. **4**, 2177 (2013).
[33] C. Guo, M. Li, J. P. Nibarger, and G. N. Gibson, Phys. Rev. A **58**, R4271 (1998).
[34] V. Tagliamonti, H. Chen, and G. N. Gibson, Phys. Rev. Lett. **110**, 073002 (2013).
[35] For reviews, see T. Seideman and E. Hamilton, Adv. At. Mol. Opt. Phys. **52**, 289 (2005); H. Stapelfeldt and T. Seideman, Rev. Mod. Phys. **75**, 543 (2003).

# Supplementary material for the manuscript "Strong field multiple ionization as a route to electron dynamics in a van der Waals cluster"

**J. Wu[1], X. Gong[1], M. Kunitski[2], F. K. Amankona-Diawuo[3], L. Ph. H. Schmidt[2], T. Jahnke[2], A. Czasch[2], T. Seideman[3], and R. Dörner[2]**

[1]*State Key Laboratory of Precision Spectroscopy, East China Normal University, Shanghai 200062, China*

[2]*Institut für Kernphysik, Goethe Universität, Max-von-Laue-Strasse 1, D-60438 Frankfurt, Germany*

[3]*Department of Chemistry, Northwestern University, 2145 Sheridan Road, Evanston, Illinois 60208, USA*

## I. Jet temperature

In molecular supersonic jet, the rotational temperature of the target could be similar to the translational temperature [s1, s2]. As demonstrated in Ref. [18], the rotational temperature of the cluster in the jet was even lower than its translational temperature. By measuring the momentum distribution of the molecular ion along the jet direction, we estimated the translational temperature of our jet to below 5K. By following this, we expect a similar or slightly higher vibrational temperature of $N_2Ar$ since the energy spacing between the lowest vibrational states is rather small, in the range of $10cm^{-1}$ [19], and therefore the vibrational modes can be efficiently cooled in the jet expansion. The $N_2Ar$ are expected to mainly populate the ground vibrational state. It consists with our observation in $Ar_2$ as demonstrated in Fig. 2(a) of Ref. [20]. A noticeable population of the high vibrational states, including the stretching and bending of the vdW bond, will reflect in a high jet temperature and increasing of the bond length as compared to the short equilibrium distance of the T-shaped ground state. Both the measured vdW bond length and the coincident momenta of the fragment ions from the direct three-body breakup indicate that the $N_2Ar$ in the jet is

mostly in its ground state T-shaped geometry.

II. Orbital calculation and population analysis

To get insight of the physical origin of the patterns observed experimentally, we here discuss the calculated orbitals of $N_2Ar$, and a population analysis which illustrates the charge distribution across the molecule in its neutral state and in the charged states studied in the main text.

The molecular orbitals were calculated using the quantum chemistry program package QChem with the coupled cluster single, doubles (triples) [CCSD(T)] method and basis set of aug-cc-pvtz and 6-311G(d,p). The $N_2Ar$ was optimized to its equilibrium T-shaped geometry, where the lengths of the N-N covalent bond and the $N_2$-Ar vdW bond were 1.0977 and 3.6956 Å, respectively.

Figures s1 and s2 show the profiles of the calculated orbitals from highest occupied molecular orbital (HOMO) to HOMO-5, illustrating that the electron density is localized about either the Ar or the $N_2$ center. Table s1 lists the corresponding orbital energies, illustrating, as expected, that the energy level spacing is small in a polyatomic molecular cluster as compared to a covalent diatomic molecule.

Complementing this information, table s2 provides a population analysis of the cluster in its neutral state and in the charged states relevant to our experiments. The charges were calculated using Mulliken, ChElPG (Charges from the Electrostatic Potential on a Grid), and NBO analysis, at the restricted Hartree Fock (RHF) level with 6-311G(d,p) basis set for the closed shell species ($N_2Ar$ and $N_2Ar^{2+}$) and unrestricted Hartree Fock (UHF) at the same basis set for the open shell species ($N_2Ar^{+}$ and $N_2Ar^{3+}$). The results agree well with our experiments regarding the sequence of the ionization events.

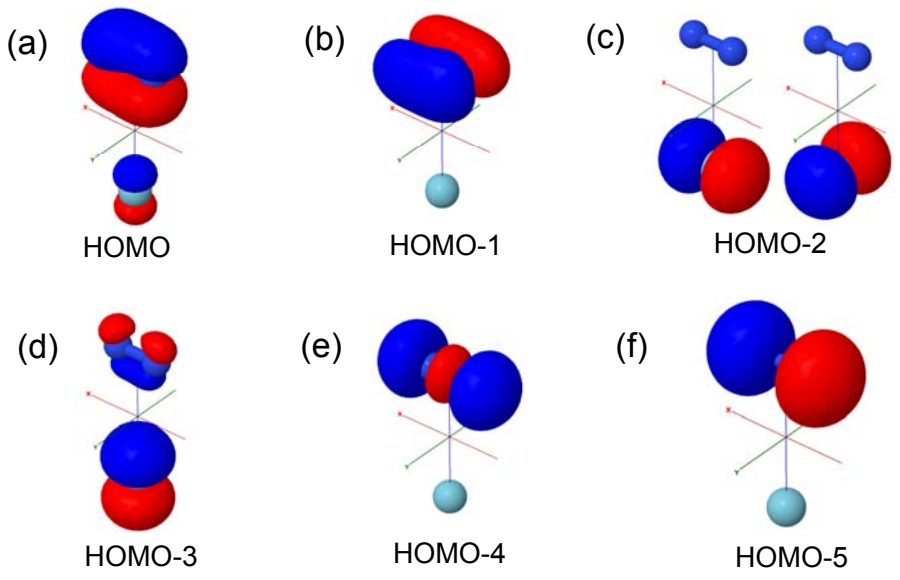


**Figure s1** Profiles of the calculated orbitals of $N_2Ar$ by using the aug-cc-pvtz basis set, where the electrons localized about either the $N_2$ (up) or the Ar (down) center.

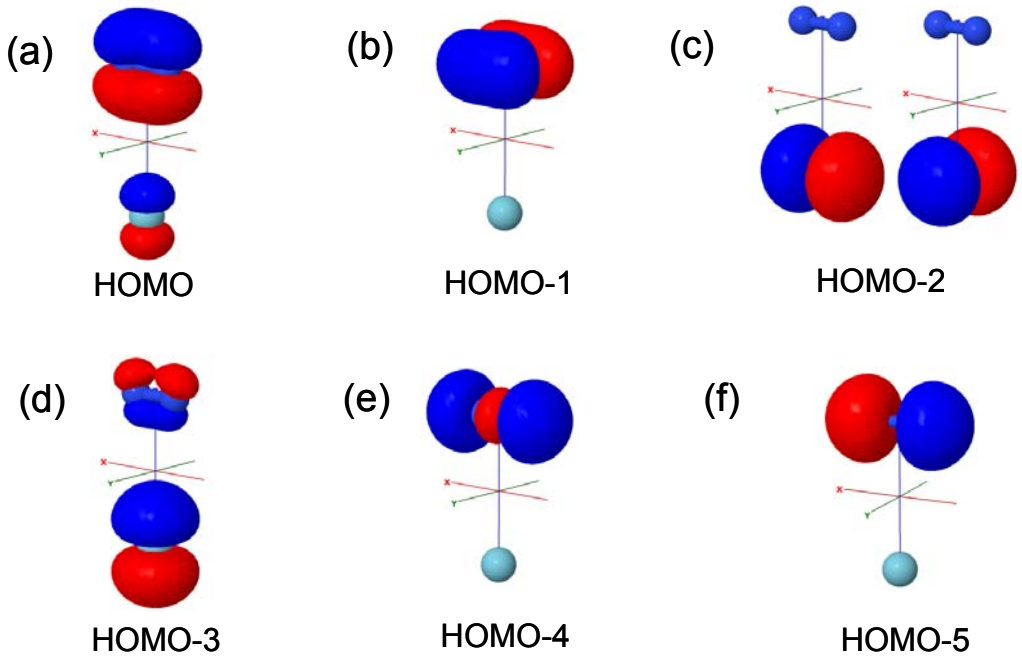


**Figure s2** Same as Fig. s2 but calculated by using the 6-311G(d,p) basis set.

| orbital | Energy (eV) aug-cc-pvtz | Energy (eV) 6-311G(d,p) |
|---|---|---|
| HOMO | -15.565 | -15.51 |
| HOMO-1 | -15.619 | -15.592 |
| HOMO-2 | -16.109 | -16.082 |
| HOMO-3 | -16.191 | -16.163 |
| HOMO-4 | -17.007 | -16.925 |
| HOMO-5 | -22.095 | -22.014 |

**Table s1** Energies of the calculated orbitals of $N_2Ar$.

| Species | Atom | Mulliken | ChElPG | NBO |
|---|---|---|---|---|
| $N_2Ar$ | N | 0.000552 | 0.001245 | 0.00005 |
| | Ar | -0.001104 | -0.002491 | -0.00010 |
| $N_2Ar^+$ | N | 0.126579 | 0.140100 | 0.12317 |
| | Ar | 0.746842 | 0.719888 | 0.75366 |
| $N_2Ar^{2+}$ | N | 0.471670 | 0.472894 | 0.47693 |
| | Ar | 1.056659 | 1.054137 | 1.04614 |
| $N_2Ar^{3+}$ | N | 0.504079 | 0.531358 | 0.50306 |
| | Ar | 1.991843 | 1.936171 | 1.99389 |

**Table s2** Charges calculated using Mulliken, ChElPG, and NBO analyses with at HF/6-311G(d,p) level of theory.

---

**References:**

[s1] I.V. Litvinyuk, Kevin F. Lee, P.W. Dooley, D.M. Rayner, D.M. Villeneuve, and P. B. Corkum, **90**, 233003 (2003).

[s2] M. Hillenkamp, S. Keinan, and U. Even, J. Chem. Phys. **118**, 8699 (2003).